Eur Biophys J (1991) 20:229–240

European Biophysics Journal


# Ion channels formed by amphipathic helical peptides

## A molecular modelling study

**Mark S. P. Sansom *, Ian D. Kerr, and Ian R. Mellor**

Department of Life Science, University of Nottingham, University Park, Nottingham, NG7 2RD, United Kingdom

Received May 24, 1991/Accepted in revised form August 19, 1991

**Abstract.** Channel forming peptides (CFPs) are amphipathic peptides, of length ca. 20 residues, which adopt an α-helical conformation in the presence of lipid bilayers and form ion channels with electrophysiological properties comparable to those of ion channel proteins. We have modelled CFP channels as bundles of parallel trans-bilayer helices surrounding a central ion-permeable pore. Ion-channel interactions have been explored via accessible surface area calculations, and via evaluation of changes in van der Waals and electrostatic energies as a $K^+$ ion is translated along the length of the pore. Two CFPs have been modelled: *(a)* zervamicin-A1–16, a synthetic apolar peptaibol related to alamethicin, and *(b)* δ-toxin from *Staphylococcus aureus*. Both of these CFPs have previously been shown to form ion channels in planar lipid bilayers, and have been shown to have predominantly helical conformations. Zervamicin-A1–16 channels were modelled as bundles of 4 to 8 parallel helices. Two related helix bundle geometries were explored. $K^+$-channel interactions have been shown to involve exposed backbone carbonyl oxygen atoms. δ-Toxin channels were modelled as bundles of 6 parallel helices. Residues Q3, D11 and D18 generate favourable $K^+$-channel interactions. Rotation of W15 about its $C\beta$-$C\gamma$ bond has been shown to be capable of occluding the central pore, and is discussed as a possible model for sidechain conformational changes in relation to ion channel gating.

**Key words:** Ion channel – Channel forming peptide – α-helix – Electrostatics

### Introduction

The past decade has seen an increase in interest in the molecular properties of receptor-gated ion channels, concomitant with an expansion of the sequence database for this superfamily of multi-subunit, trans-membrane proteins. As yet, it has not proved possible to obtain high resolution structural data for any of these proteins. However, considerable insights into the molecular nature of the central pore region of channel proteins have been gained from studying simple model systems, namely channel forming peptides (CFPs; Sansom 1991).

CFPs are short (ca. 20 residues) hydrophobic peptides which are believed to adopt an α-helical conformation in the presence of lipid bilayers (e.g. Vogel 1987). A transmembrane voltage induces them to form ion channels in bilayers, of comparable functional properties (conductance, ion selectivity etc.) to those generated by channel proteins. Channels are formed by a process of self-assembly within the plane of the bilayer which generates bundles of parallel trans-membrane helices (Boheim et al. 1983). These helices surround a central pore, which is lined by hydrophilic sidechains, thus permitting permeation of selected ions. A major reason for studying CFPs is that it is feasible to attempt to relate their functional (i.e. electrophysiological) properties to structural (NMR and/or X-ray diffraction) data in order to develop models of channel structure. This paper describes a methodology for modelling CFP channels, alongside its application to two examples of CFPs which have been studied in the authors' laboratory.

The first CFP to be considered is zervamicin-A1–16 (Zrv-A1–16):

*t*Boc-W-I-A-U-I-V-U-L-U-P-A-U-P-U-P-F-OMe

(In this and subsequent sequences the standard one letter code is used, with the addition of $U$ = α-amino isobutyric acid. *t*Boc is an N-terminal *t*-butoxycarbonyl group, and the C-terminus is blocked by a methyl ester.) Zrv-A1–16 in one of the family of peptaibol CFPs, of which the best known example is alamethicin. Zrv-A1–16 is an apolar synthetic derivative of the naturally occurring zervamicins (Krishna et al. 1990). The single channel properties of Zrv-A1–16, and of the related polar CFPs Zrv-IIB and Zrv-Leu have been studied using planar bilayer techniques (Agarwalla et al. 1991; Balaram et al. 1991; Sansom 1991). Importantly, from the point of view of modelling studies, the crystal structure of Zrv-A1–16 has

* *Present address and address for offprint requests:* Laboratory of Molecular Biophysics, University of Oxford, The Rex Richards Building, South Parks Road, Oxford, OX1 3QU, United Kingdom

been determined at 0.91 Å resolution (Karle et al. 1987). As discussed in more detail below, Zrv-A1–16 forms a kinked helical structure, which is functionally amphipathic despite the overall apolar nature of the peptide.

The other CFP we discuss is δ-toxin from *Staphylococcus aureus*. This is a 26 residue peptide:

f-M-A-Q-D-I-I-S-T-I-G-D-L-V-K-W-I-I-D-T-V-N-K-F-T-K-K

the physico-chemical properties of which have been extensively characterised (Fitton 1981). It has been shown to form cation selective channels in planar lipid bilayers, and the properties of these channels have been studied in some detail (Mellor et al. 1988; Sansom and Mellor 1990; Sansom 1991). Preliminary crystallographic studies have been reported (Thomas et al. 1986), but a full structure determination is still awaited. High resolution NMR studies in the presence of phospholipid micelles (Lee et al. 1987) and in solution in methanol (Tappin et al. 1988) have provided evidence for a largely α-helical conformation.

The studies described in this paper constitute an exploration of an uncomplicated approach to modelling CFP channels. An attempt is made to rationalize the observed properties of CFP channels using such models. In particular, studies of channel-cation interactions are described. Related studies in this field have been carried out by Furois-Corbin and Pullman (1989a, b, 1991), and by Eisenman and Alvarez (1991). Both of these groups have focused their attention on modelling the central pore region of the nicotinic acetylcholine receptor (nAChR). An advantage of modelling CFP channels is that structural data is available for the constituent monomer, even if not for the helix bundle as a whole.

## Methods

Our overall approach to modelling CFP helix bundles consists of three stages: obtaining a structure for the CFP monomer; generating a helix bundle; and evaluating interaction energies between the helix bundle model and a $K^+$ ion as a function of the position of the ion within the pore. Details of the monomer structures employed are given below. The focus here is on general aspects of the latter two procedures.

### *Generation of helix bundles*

All modelling was carried out using QUANTA 3.0 (Polygen, Waltham, MA), run on a Silicon Graphics (Mountain View, CA) Personal Iris 4D25T workstation. Energy minimization and empirical energy function calculations were performed using the molecular mechanics program CHARMm (V21; Brooks et al. 1983). All auxiliary programs were written in Fortran77.

Helix bundle generation was carried out using the program *bndlq*, the principles of which are illustrated in Fig. 1. In the stage A, the helix of the monomer is aligned parallel to the *z*-axis, such that the centre of the helix lies at the origin of the coordinate system. For example, for a regular 20 residue α-helix, the helix centre may be defined by the midpoint of the Cα atoms of residues 1–20, and the helix axis by the unit vector from the helix centre to the midpoint of the Cα atoms of residues 17 to 20. Having aligned the helix, it is rotated about the helix axis (i.e. about the *z*-axis) by an angle θ such that the centre of the hydrophilic face of the helix points along the *x*-axis (Fig. 1A). The value of θ is determined via interactive inspection of the helix viewed down the *z*-axis, although one might attempt to define θ less subjectively via calculation of the hydrophobic moment of the CFP sequence (Eisenberg et al. 1982, 1984). Having oriented the helix thus, in stage B a parallel helix bundle is generated (Fig. 1B). The parameters determining the bundle geometry are the number of helices/bundle (*N*) and the inter-axial separation of the constituent helices (*R*). The helices of the bundle are oriented such that helix-1 is always positioned with its hydrophilic face pointing along the *x*-axis, and with the axis of the pore lying along the *z*-axis. Thus movement along the *z*-axis corresponds to movement along the centre of the pore.

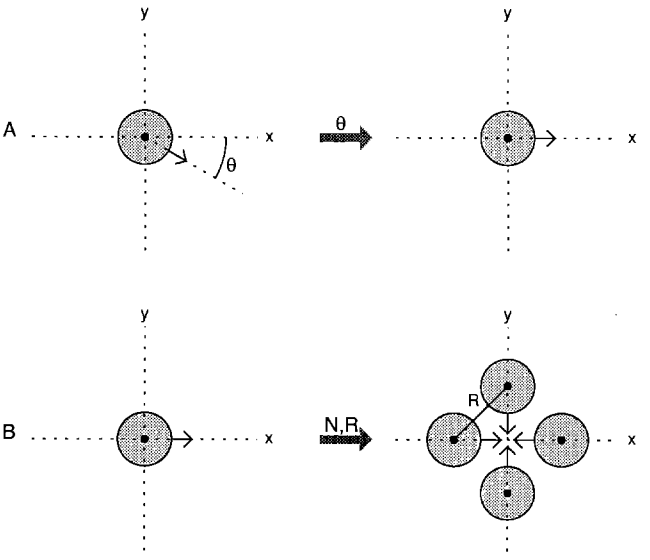


**Fig. 1 A, B.** Schematic diagram of the parameters determining the geometry of helix bundle formation. **A** shows rotation of the helix about its axis (*z*) through an angle θ, such that the centre of the hydrophilic face of the helix (*represented by an arrow*) is directed along the *x*-axis. **B** shows generation of a parallel helix bundle of *N* helices, with an inter-axial separation *R*. Note that each helix is rotated so that the centre of the hydrophilic face is directed towards the centre of the pore (i.e. the *z*-axis)

After generation of the initial bundle model, unfavourable (i.e. overlapping) contacts between sidechains at the helix-helix interfaces were relieved by interactive adjustment of sidechain torsion angles. Finally, the resultant structure was subjected to at least 50 cycles of steepest descents energy minimization, using CHARMm, so as to optimize local interactions between sidechain atoms by relieving bad van der Waals contacts and strained bond lengths and angles. No constraints were imposed on atomic movements during the minimization. The final structure was used as the basis for calculations of bundle-ion interaction energies.

*$K^+$ profiles*

The aim of these calculations is to probe for potential interaction sites between a $K^+$ ion moving through the central pore and the atoms lining the pore. It was not the intention to calculate a true permeation profile for the ion, as the model does not incorporate water, and so cannot take into account solvation/desolvation energies of the ion. However, by identifying potential interaction sites between the ion and the channel model, the approach adopted provides useful insights into the design of CFP channels, as will be seen below.

The channel model was treated as a rigid body, and a $K^+$ ion translated along the central ($z$) axis of the pore, evaluating the empirical energy of interaction of the ion and the channel as a function of $z$. The potential energy function ($E_T$) used is the sum of a van der Waals ($E_V$) and an electrostatic ($E_E$) term:

$$E_T = E_V + E_E$$

The van der Waals energy is given by a Lennard-Jones 6–12 potential function:

$$E_V = \sum_{ij} \left( \frac{A_{ij}}{r_{ij}^{12}} - \frac{B_{ij}}{r_{ij}^{6}} \right) sw\,(r_{ij})$$

where *sw* is a switching function (Brooks et al. 1983), with a cutoff distance of 20 Å. The electrostatic energy is given by:

$$E_E = \sum_{ij} \left( \frac{q_i\, q_j}{4\pi\, \varepsilon_0\, r_{ij}^2} \right) sh\,(r_{ij})$$

where *sh* is a shift function (Brooks et al. 1983), with a cutoff distance of 20 Å. For both energy terms the non-bonded list cutoff was 21 Å. Note that the electrostatic energy is calculated using a distance dependent dielectric, i.e. $\varepsilon = \varepsilon_0\, r$, (Brooks et al. 1983, 1988; Rogers 1986) in order to mimic the effect of solvent-screening on ion-channel interactions at larger distances. The van der Waals parameters and the partial charges of the constituent atoms ($q_i$) were taken from the CHARMm parameter set PARM20.

## Results

*Zervamicin A1–16*

*Monomer structure.* The crystal structure of monomeric Zrv-A1–16 has been determined by Karle et al. (1987). This structure (see Fig. 2) was used as the basis for further modelling. Before proceeding it is of value to examine some aspects of the monomer structure in more detail. As in alamethicin, the structure of Zrv-A1–16 is divided into two helical segments by a proline (P10) induced kink. Zrv-A1–16 has no polar sidechains. However, a functionally amphipathic structure is generated via exposure of two backbone carbonyl oxygen atoms, O7 and O14. These lie on the same (convex) face of the molecule, and do not participate in intramolecular H-bond formation. As can be seen from Table 1, O7 and O14 are both solvent accessible, as are two carbonyl oxygens (O15 and O16) at the C-terminus of the molecule. Thus this apparently apolar peptide has four carbonyl oxygen atoms exposed to solvent, which are therefore potentially available for peptide-ion interactions in transbilayer helix bundles. It

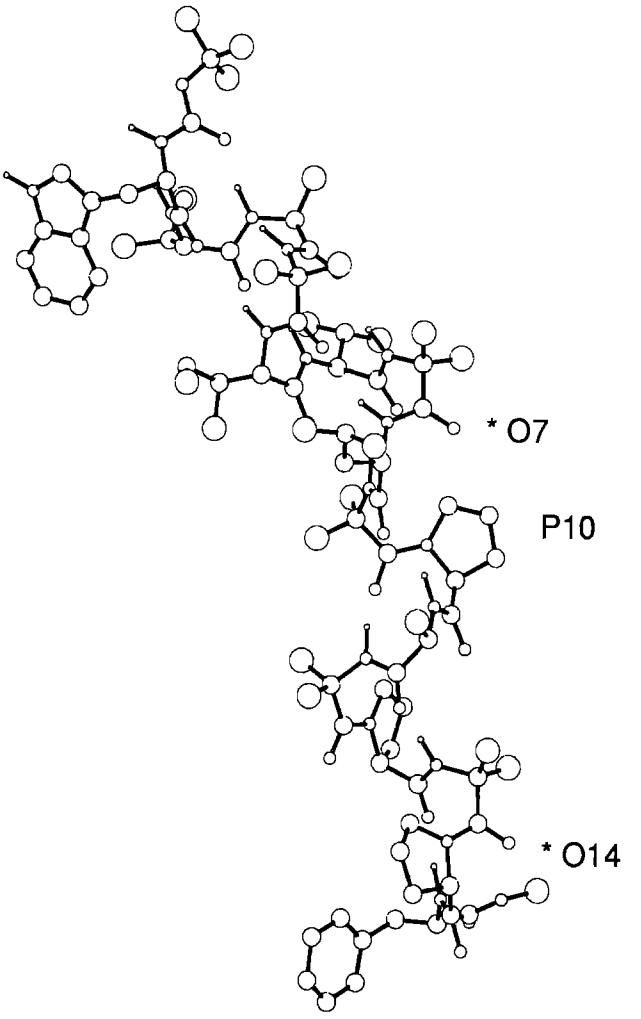


**Fig. 2.** Structure of a Zrv-A1–16 monomer (Karle et al. 1987), oriented such that the C-terminal helix is approximately vertical. In this, and subsequent, diagrams only those hydrogen atoms bonded to non-carbon atoms are shown. The position of the kink-inducing proline (P10) and of the carbonyl oxygens (*O) of residues 7 and 14 are indicated

**Table 1.** Zrv-A1–16 solvent accessible surface areas. Solvent accessible surface areas, calculated using a probe radius of 1.4 Å, are shown for the carbonyl oxygens which line the pore formed in model A Zrv-A1–16 helix bundles (O7 and O14), and for the exposed carbonyl oxygens at the C-terminus of the helix (O15 and O16). The areas are listed for the Zrv-A1–16 monomer, and for $N=4$, 6, and 8, model A bundles

| Atom | Solvent monomer | Accessible $N=4$ | Surface $N=6$ | Area (Å$^2$) $N=8$ |
|---|---|---|---|---|
| O7 | 13 | 3 | 7 | 9 |
| O14 | 11 | 2 | 4 | 6 |
| O15 | 30 | 20 | 21 | 22 |
| O16 | 24 | 24 | 16 | 15 |

should be noted that backbone carbonyl oxygen-metal ion interactions have been observed in a number of protein structures (Chatrabarti 1990). The total solvent accessible surface area of Zrv-A1–16 is 1 944 Å$^2$, of which 104 Å$^2$ is polar. Thus, the four exposed carbonyl oxygens make up 75% of the polar surface of the monomer.

*Model A and model B helix bundles.* Two alternative classes of models of helix bundles formed by Zrv-A1–16 have been explored. In the first class (model A) the *C-terminal* helices of the peptides are parallel to one another. The rotation angle, $\theta = 170°$, about the axis of the C-terminal helix was selected so that the hydrophilic face (defined by atoms O7 and O14) pointed along the $x$-axis. The inter-axial separation of the C-terminal helices was set to 9.5 Å. This resulted in close apposition between the helices, without an excessive number of overlapping contacts of sidechain atoms. Previous experimental studies on Zrv-IIB channels formed in planar lipid bilayers (Balaram et al. 1991; Sansom 1991) have indicated that symmetrical helix bundles are formed for $N = 4$ to 8, and so helix bundles were modelled for the same range of values of $N$. For each $N$, overlapping contacts between sidechain atoms were relieved by interactive rotation of the sidechains of V6 residues about their C$\alpha$-C$\beta$ bonds, and of L8 residues about their C$\alpha$-C$\beta$ and C$\beta$-C$\gamma$ bonds. Finally, each bundle order was subjected to 50 cycles of unconstrained energy minimization. Comparison of the resultant constituent monomers with the initial structure of the monomer revealed relatively minor changes in atomic positions other than for the V6 and L8 sidechains.

Model B helix bundles were constructed with the *N-terminal* helices aligned parallel to one another. Otherwise, the procedure was similar to that for model A, i.e. the initial helix was oriented such that its hydrophilic face pointed along the $x$-axis ($\theta = 0°$), and the bundles constructed with $R = 9.5$ Å and $N = 4$ to 8. As with model A, torsion angle adjustments of V6 and L8 were required prior to 50 cycles of energy minimization.

Figure 3 illustrates $N = 4$ and $N = 6$ for bundles for model A, viewed along the $z$-axis. The N-terminal tryptophan residues are clearly visible, directed away from the central pore towards the surrounding bilayer region. The sidechains lining the pore (A3, U4, U7, P10, A11, U14 and P15) are, on average, less bulky than those located at the helix-helix interface or directed towards the bilayer (W1, I2, I5, V6, L8, U9, U12, P13, F16). Figure 4 shows space-filling diagrams of the same model A bundles. These are viewed along the $y$-axis, and only two monomers are shown, namely those whose centres lie opposite one another on the $x$-axis. Thus these diagrams correspond, approximately, to $x$ $z$-plane sections through the bundle, i.e. sections cut vertically through the centre of the pore. The funnel shape of the pore is evident, with the wider mouth of the funnel corresponding to the N-termini of the peptides. For $N = 4$ (6) the van der Waals radius of the N-terminal mouth of the pore is ca. 7.6 Å (10.4 Å), and the radius of the C-terminal mouth of the pore is ca. 2.6 Å (5.1 Å). Carbonyl oxygens O7 and O14 are shaded. They are both directed towards the centre of the pore. Evaluation of solvent accessible surface areas (Table 1) for model A bundles reveals that although the accessibility of these atoms is reduced relative to that in the isolated monomer, both O7 and O14 are accessible even in the $N = 4$ bundle. Their accessibility increases as $N$ increases. The C-terminal carbonyl oxygens (O15 and O16) remain exposed for all values of $N$.

Model B also results in a funnel shaped pore, as can be ssen by reference to Fig. 5 where the $N = 4$ bundles for

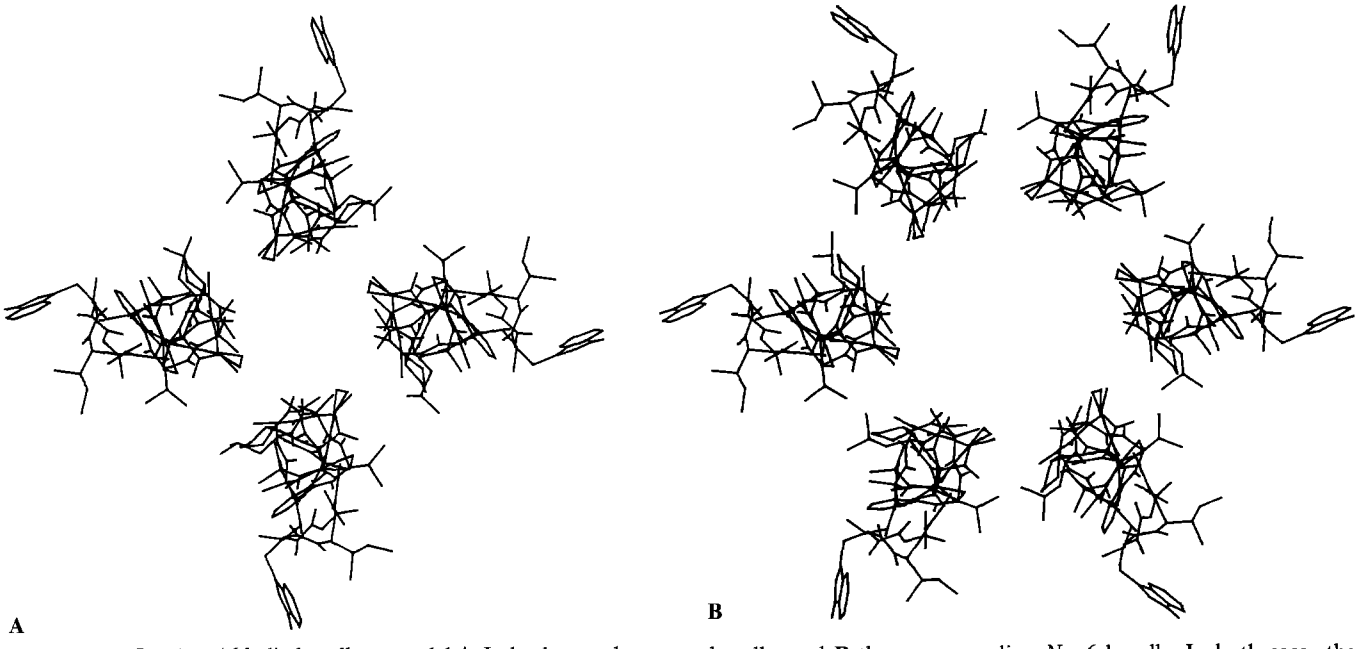

**Fig. 3 A, B.** Zrv-A1–16 helix bundles – model A. In both cases bundles are constructed with parallel C-terminal helices, with an inter-axial separation of $R = 9.5$ Å, and are viewed down the $z$-axis (i.e. down the axis defined by the centre of the pore). **A** shows the $N = 4$ bundle, and **B** the corresponding $N = 6$ bundle. In both cases the N-terminal tryptophan sidechain is clearly visible, pointing away from the bundle

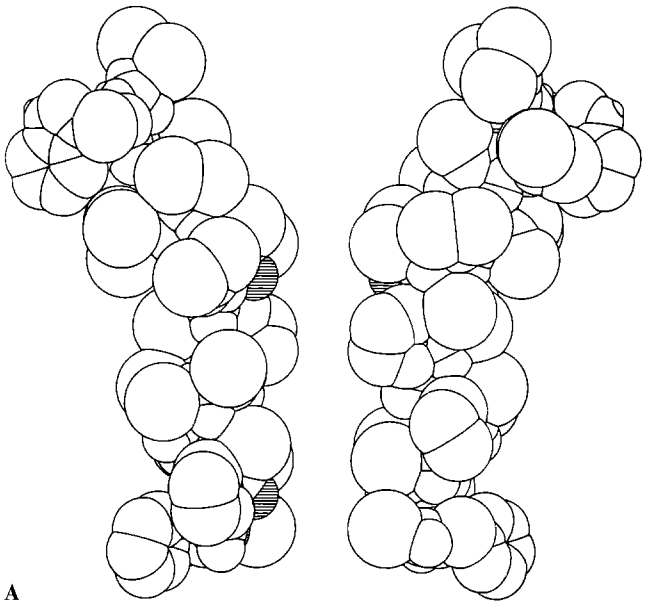

A

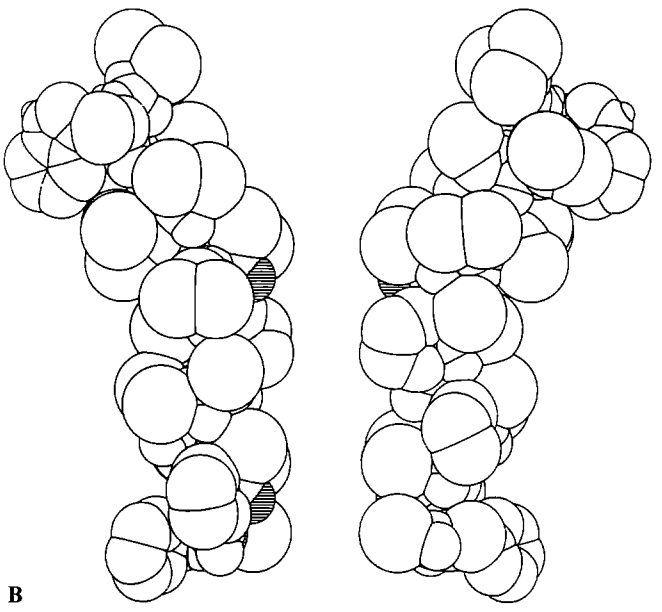

B

**Fig. 4A, B.** Sections through Zrv-A1–16 bundles – model A. In both cases the pair of helices whose axes intersect the $x$-axis and which are on opposite sides of the pore are shown, viewed along the $y$-axis. Atoms are represented by spheres with radii proportional to their van der Waals radii. In the case of carbon atoms, whose attached hydrogen atoms are not explicitly included, the radii of the corresponding extended atom representations are used. The carbonyl oxygens of residues 7 (*midway down pore*) and 14 (*bottom of pore*) are shaded. A funnel shaped pore is seen, with the N-terminal tryptophan sidechains at the top of the diagrams. **A** shows the $N=4$ and **B** the corresponding $N=6$ bundle

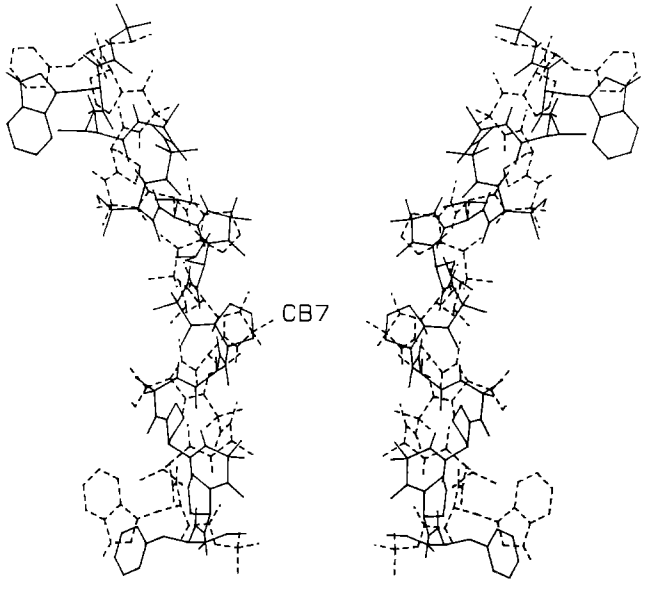


**Fig. 5.** Comparison of Zrv-A1–16 $N=4$ bundles, model A vs. model B. The solid lines represent model A (Figs. 3A and 4A) in which the C-terminal helices are parallel, with the C-termini at the bottom of the diagram. The broken lines represent model B, in which the N-terminal helices are parallel, with the N-termini at the bottom of the diagram. The view is along the $y$-axis. The overall funnel shape of the pore is retained in both models. Model B has the central pore partially occluded by the C$\beta$1 atoms of the four U7 residues, one of which is labelled (CB7)

models A and B are superimposed. For $N=4$ (6) the C-terminal pore radius of model B is ca. 7.7 Å (10.4 Å), and the N-terminal radius is ca. 1.0 Å (3.8 Å). As in model A, model B results in the two aromatic sidechains being directed towards the surrounding bilayer, and O7 towards the centre of the pore. The major difference between the two models lies in the location of the sidechain C$\beta$1 atoms of residue U7. In model A these are directed up towards the mouth of the funnel shaped region, whereas in model B they are at the beginning of the narrower region of the pore, and thus form a constriction. In model B, $N=4$ this constriction (labelled CB7 in Fig. 5) occludes the pore (see below). This is not the case for the higher $N$ model B bundles.

*$K^+$-profiles.* The empirical energy of interaction between a $K^+$ ion translated along the $z$-axis, from $z=-40$ Å to $+40$ Å, and the peptide channel was evaluated for both model A (Fig. 6A and 7A) and model B (Fig. 6B and 7B) bundles. Figure 6A depicts the results of such calculations for the $N=4$ model A bundle. The N-termini of the helices correspond to the left-hand side of the diagram ($z=-21.3$ Å) and the C-termini correspond to the right-hand side ($z=+10.6$ Å). The van der Waals interaction energy is favourable for most of the length of the channel, forming a broad, shallow potential well. This reflects the close interactions of the ion with the atoms lining the pore of the $N=4$ bundle. However, the total energy of interaction is dominated by the electrostatic term. This exhibits two well defined potential minima. The positions of these minima correspond to the locations, on $z$, of the two exposed carbonyl oxygens discussed above – O7 at $z=-7.3$ Å and O14 at $z=+6.3$ Å. It is possible that the helix dipoles (equivalent to a formal charge of ca. $-1/2$ at the C-terminus and $+1/2$ at the N-terminus of an $\alpha$-helix Hol et al. 1978) contributes to the well at $z=+8$ Å. A corresponding barrier resulting from the helix dipoles at the N-termini is not seen as a result of the non-parallel arrangement of the N-terminal helices, and the compen-

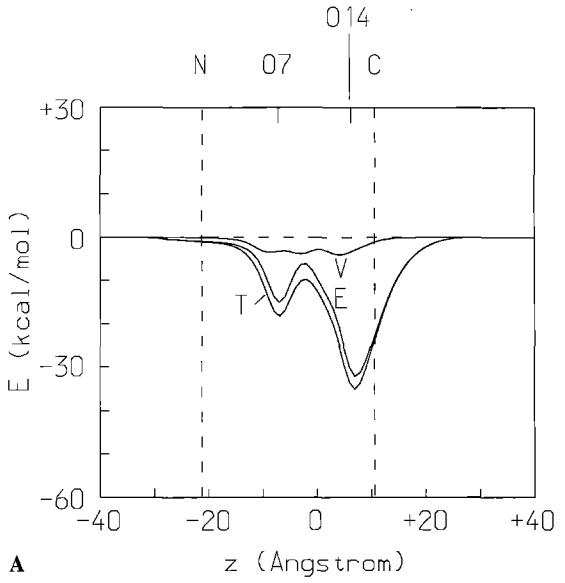


A

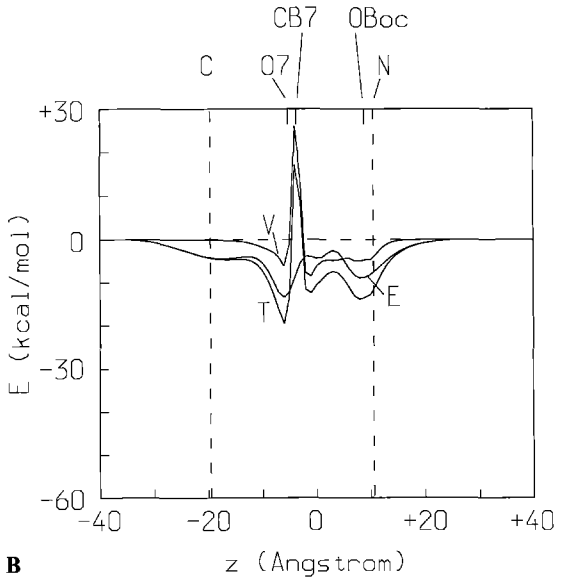


B

**Fig. 6 A, B.** $K^+$ profiles for Zrv-A1–16 $N=4$ bundle models. **A** corresponds to model A, in which the C-terminal helices are parallel (Figs. 3 A and 4 A), whereas **B** corresponds to model B, in which the N-terminal helices are parallel (Fig. 5). The interaction energy between the ion and the helix bundle is shown as a function of distance along the pore axis ($z$). Note that negative values of $z$ correspond to the top of the pores shown in Figs. 4 and 5, whereas positive values of $z$ correspond to the bottom of the diagrams. The approximate positions of the N- and C-termini are indicated by vertical broken lines. The positions along $z$ of the following atoms are also indicated: OBoc – ester oxygen of N-terminal *t*Boc blocking group; O7 – carbonyl oxygen of residue 7; CB7 – C$\beta$1 atom of residue 7; and O14 – carbonyl oxygen of residue 14. V, E and T represent the van der Waals, electrostatic and total interaction energies respectively

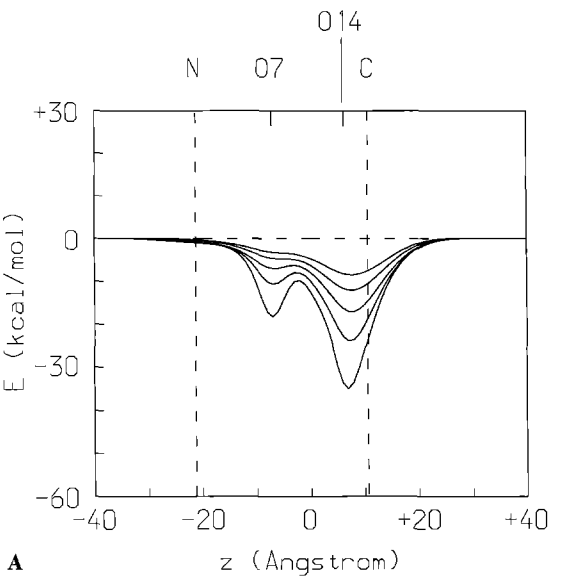


A

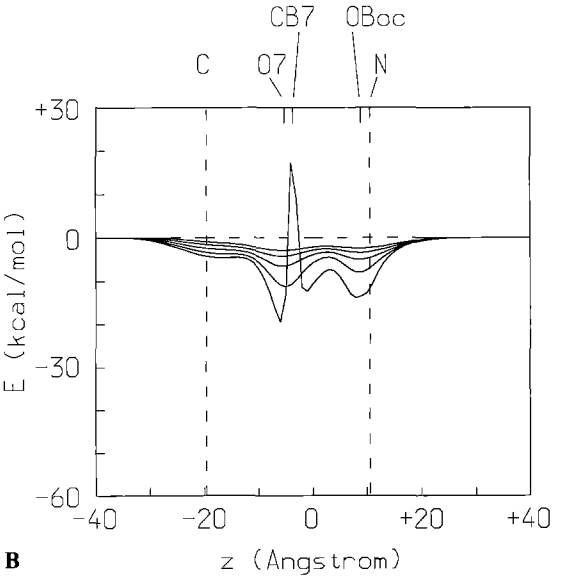


B

**Fig. 7 A, B.** $K^+$ profiles for Zrv-A1–16 $N=4$ to 8 bundles. **A** corresponds to model A bundles, whereas **B** corresponds to model B bundles. In both cases the total interaction energy is shown, for $N=4$ (*lower curves*) to $N=8$ (*upper curves*). The positions along $z$ of non-carbon atoms lining the pores are indicated as in Fig. 6

satory effect of the partial negative charge on the ester oxygen of the *t*Boc group (see below). Overall, the model A $N=4$ profile supports the proposal, made on the basis of surface accessibility calculations that O7 and O14 can provide favourable ion-channel interactions.

The corresponding profiles for the model B $N=4$ bundle are shown in Fig. 6 B. Here the C-termini of the helices are on the left-hand side ($z=-19.6$ Å) and the N-termini on the right ($z=+10.5$ Å). The van der Waals interaction energy generates a broad well, interrupted by a high barrier coincident with the position ($z=-3.7$ Å) of the C$\beta$1 atoms of U7. At this point along the pore axis the C$\beta$1-C$\beta$1 separation is 5.4 Å, corresponding to a van der Waals radius for the pore of only 0.3 Å. Thus it is not surprising that there is a strong repulsive interaction if one attempts to locate a $K^+$ ion (radius 1.33 Å) in such a hole. The electrostatic energy profile for model B is somewhat more complex than that for model A. However, the overall profile is dominated by the van der Waals barrier and so discussion of the electrostatics is provided below in the context of higher $N$ channels. Overall, empirical energy function calculations confirm the impression gath-

ered from inspection of model B, $N=4$ that the sidechains of U7 occlude the pore.

The total interaction energy profiles for model A $N=4$ to 8 are given in Fig. 7A. For $N \geq 5$, the profiles are dominated by the electrostatic terms, the van der Waals interactions being relatively small. In all cases the pair of potential minima generated by O7 and O14 are evident. The minima become shallower and less well defined as $N$ increases, paralleling the increase in O7 (O14)-$K^+$ separations, equal to 4.3, 5.7, 7.0, 8.6 and 10.0 Å (4.2, 5.6, 7.0, 8.4 and 9.9 Å) for $N=4$ to 8. The corresponding set of interaction energy profiles for model B is shown in Fig. 7B. The barrier generated by C$\beta$1 of U7 is only present for the $N=4$ profile. For $N \geq 5$ a broad multi-well potential is seen, which is due almost entirely to electrostatic interactions. A broad minimum is seen in the region of the C-terminus, representing the effects of ion-O14 interactions. These are weakened relative to model A, because the ion-O distances are increased. The main potential well corresponds to O7, at $z=-5.3$ Å. As for model A this well becomes shallower as $N$ increases. Note that the O7-$K^+$ separations for model B (4.3, 5.6, 7.0, 8.4 and 9.9 Å for $N=4$ to 8) are almost identical to those for model A (see above). A second, shallower, well corresponds to the position of the ester oxygen of the N-terminal *t*Boc group ($z=+8.9$ Å). In this case the O-K distances are somewhat greater than in model A (5.8, 7.2, 8.6, 10.1 and 11.5 Å for $N=4$ to 8), which may contribute to the weakened ion-peptide interactions.

Overall, it can be seen that model A generates a pore permeable to $K^+$ ions for all values of $N \geq 4$, with a potential profile characterised by two distinct wells, whereas model B generates a pore only for $N \geq 5$, with rather broad, shallow potential profiles without such clearly defined minima.

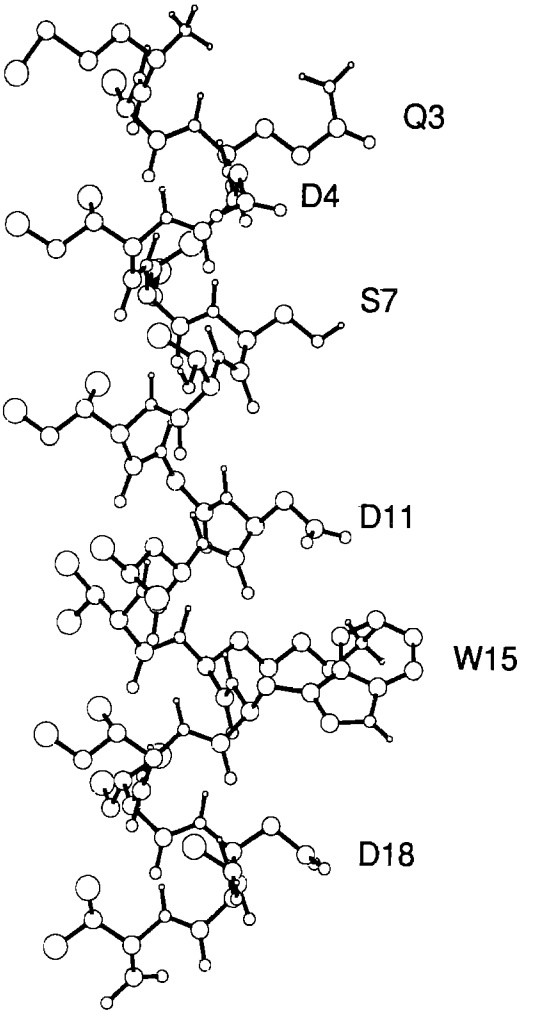


**Fig. 8.** α-Helical model of the δ-toxin-1–20 monomer. The approximate positions of principal hydrophilic sidechains are labelled

*δ-Toxin-1–20*

*Monomer structure.* NMR studies (Tappin et al. 1988) have shown that, when dissolved in methanol, the first 20 residues of δ-toxin are in an α-helical conformation, whereas the C-terminal hexapeptide is largely disordered. Thus, as a first step towards modelling the channels formed by δ-toxin (Mellor et al. 1988), residues 1 to 20 were constructed as a regular α-helix with sidechains in extended conformations. The N-terminus was blocked with a formyl group, as in the native toxin, and the C-terminus blocked with an amide group. Inspection of a helical wheel plot of the sequence of δ-toxin-1–20 (Sansom 1991) revealed the helix to be highly amphipathic, with clearly separated hydrophobic and hydrophilic faces. Figure 8 shows the model for the δ-toxin-1–20 monomer, with the polar sidechains, forming a "hydrophilic strip" on one side of the helix, labelled: Q3, D4, S7, D11, W15 and D18. The opposite, hydrophobic face of the helix is composed largely of V, L and I residues.

*$N=6$ bundle model.* Analysis of the concentration dependence of channel formation in planar lipid bilayers (Mellor et al. 1988) suggests that $N=6$ helix bundles are a major component of δ-toxin channels. Furthermore, given that channels form readily when δ-toxin is only present on one side of the bilayer, it is likely that *parallel* α-helices surround the central pore of the bundle. Accordingly, a parallel, $N=6$ bundle model of δ-toxin-1–20 was constructed.

The rotation of the helix about the $z$-axis ($\theta=180°$) was such that the hydrophilic strip of residues (above) was directed along the $x$-axis. $R$ was set to 10 Å in order to maximize helix-helix interactions, whilst minimizing overlaps between sidechain atoms of adjacent helices. In the initial model thus generated the sidechains of W15 occluded the central pore. The channel was "opened" by rotating the W15 rings by 180° about their C$\beta$-C$\gamma$ bonds. The sidechains of the K14 residues were also altered, by interactive rotations about torsion angles, so as to unblock the pore and to prevent steric conflicts. Finally, the N- and C-terminal blocking groups were rotated to their lowest potential energy conformations. This modified model was then subjected to 50 cycles of unconstrained energy minimization to yield the final $N=6$ bundle used in all further calculations. A view of the final model is shown in Fig. 9A, viewed down the $z$-axis.

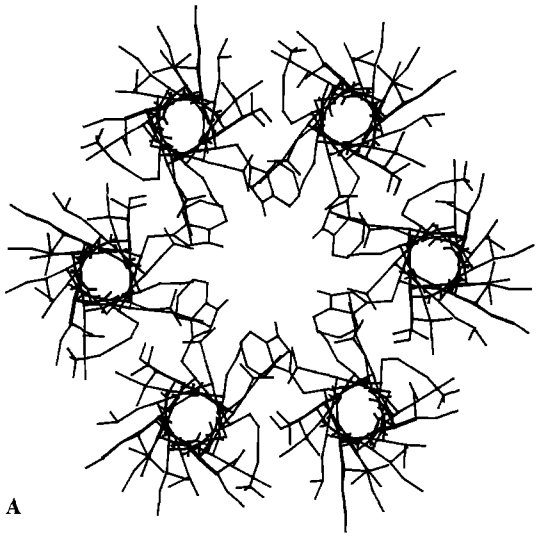

A

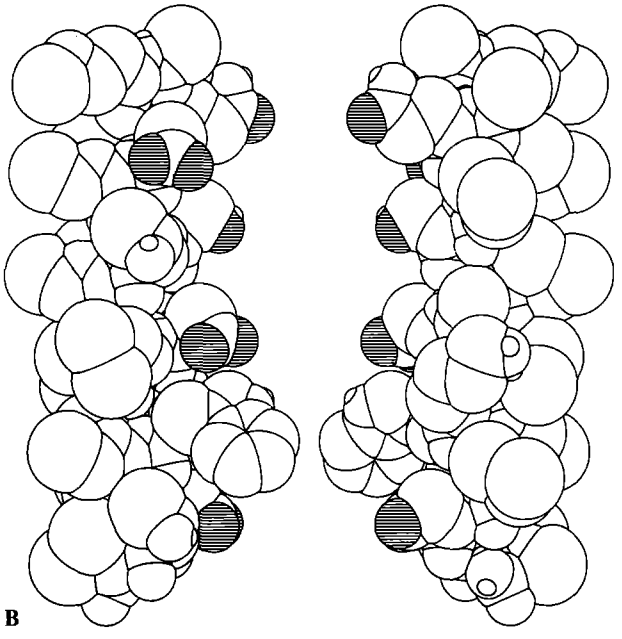

B

**Fig. 9 A, B.** $N=6$ model of a $\delta$-toxin-1–20 helix bundle. The helices are parallel, with an interaxial separation of $R=10$ Å. The W15 sidechains are clearly visible in the view down the $z$-axis (**A**). **B** shows a space-filling representation of the same model viewed down the $y$-axis. The oxygen atoms of the sidechains of residues Q3, D4, S7, D11 and D18 are shaded

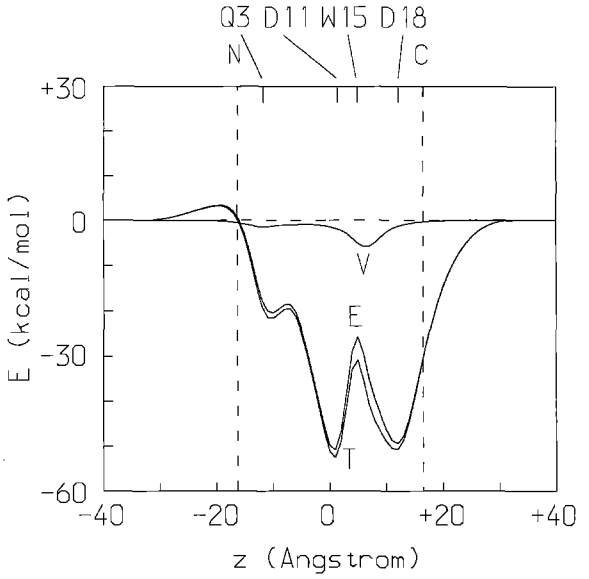


**Fig. 10.** $K^+$ profile for the $N=6$ $\delta$-toxin-1–20 model. The representation is the same as in Figs. 6 and 7, with the positions on $z$ of the following atoms labelled: Q3-Q3 : Oε1; D4-D4 : Oδ1; D11-D11 : Oδ1; W15-W15 : Hε1; and D18-D18 : Oδ1

**Table 2.** $\delta$-Toxin-1–20 solvent accessible surface areas. Solvent accessible surface areas were calculated for *polar* atoms (i.e. O and N atoms, and H atoms available for H-bonding) of the $\delta$-toxin sidechains of the residues forming the "hydrophilic strip". Areas were calculated for the isolated monomer, and for the equivalent atoms within the $N=6$ helix bundle. The total area of the isolated monomer is 2305 Å$^2$, of which 463 Å$^2$ is contributed by polar atoms. The equivalent areas of the monomer as part of an $N=6$ bundle are 1383 Å$^2$ and 205 Å$^2$ respectively. Thus, 55% of the polar surface of the monomer is buried upon bundle formation

| Residue | Solvent accessible monomer | Surface area (Å) $N=6$ |
|---|---|---|
| Q3 | 77 | 29 |
| D4 | 69 | 6 |
| S7 | 37 | 34 |
| D11 | 59 | 14 |
| W15 | 22 | 6 |
| D18 | 79 | 26 |

Solvent accessible surface areas were calculated for the polar sidechain atoms of the residues constituting the hydrophilic strip, both for the isolated monomer and for the monomer as a component of the $N=6$ bundle (Table 2). From these it is evident that whereas the sidechain atoms of Q3, S7, D11 and D18 are still largely exposed in the bundle, those of D4 are largely buried. Inspection of the model shows that D4 is directed away from the central pore, towards the helix-helix interface region. Overall, ca. 55% of the polar surface area of the monomer is buried upon $N=6$ bundle formation. If one examines a space-filling representation of two opposing monomers of the helix bundle, viewed from along the $y$-axis (Fig. 9 B), it is evident that the sidechains of Q3, S7, D11 and D18 line the central pore. It is also evident that the sidechain of W15 is oriented such that its Nε1 and Hε1 atoms are directed towards the centre of pore. Calculations of accessible surface areas confirm that these atoms remain (partially) exposed in the helix bundle. Thus, the pore is lined by two rings of negatively charged residues, at positions 11 and 18, plus two rings of neutral polar residues, at positions 3 and 7, and is constricted in the region of residue 15.

*$K^+$ profile.* The empirical $K^+$ ion-channel interaction energy was evaluated from $z=-40$ to $+40$ Å (Fig. 10). The profile extends from just to the left of the N-termini of the helices ($z=-16.3$ Å) to beyond the right of the C-termini

($z = +16.5$ Å). There is a slight barrier at the N-terminus, which arises from the dipoles of the parallel helices, but this is lower than would be otherwise be the case (MSPS, unpublished results), as a result of partial cancellation by negative charge on the sidechains of D4 (at $z = -9.1$ Å). There are three minima in the overall profile, corresponding to the positions of the sidechains of Q3 ($z = -11.9$ Å), D11 ($z = +1.3$ Å), and D18 ($z = +12.0$). The minimum associated with D18 is broadened towards the C-terminus as a result of favorable interactions with the helix dipoles.

If one examines the individual components of the profile, it is evident that there is a minimum in $E_V$ which corresponds to the position of the W15 sidechain ($z = +4.8$ Å). As discussed above, this region is characterised by a constriction of the pore. Indeed, at its narrowest point, the $K^+$-W15 : H$\varepsilon$1 separation is only 3.2 Å – hence the favourable van der Waals interactions. Indeed, if the W15 rings are flipped 180° about their C$\beta$-C$\gamma$ bonds (i.e. back to their conformation in the initial model), then the $K^+$-W15 separation is such that the pore is occluded. Examination of the $E_E$ profile confirms that the minima in the $E_T$ profile result primarily from electrostatic interactions. The corresponding $K^+$-sidechain atom approach distances are 4.9 Å for Q3 : O$\varepsilon$1, 4.8 Å for D11 : O$\delta$1 and 6.3 Å for D18 : O$\delta$1. It is interesting to note that the close approach of $K^+$ to W15 : H$\varepsilon$1 results in a barrier in the profile as a result of the unfavourable interaction between $K^+$ and the partial positive charge on the H atom.

Overall, it can be seen that the $\delta$-toxin-1–20 $N = 6$ channel model is organized such that the sidechains of the hydrophilic strip provide favourable interaction sites for a permeant cation. This correlates with the observed selectivity of $\delta$-toxin channels for cations over anions (Mellor et al. 1988).

## Discussion

### *Helix bundle modelling*

The approach described for modelling CFP helix bundles is dependent upon input of key parameters ($\theta$, $N$, $R$) by the user. The values of these parameters are determined by a combination of consideration of the general properties of amphipathic helices ($\theta$), experimental estimation from planar bilayer studies ($N$), and interactive adjustment ($R$). One should question the extent to which this is justified, and explore how one might improve upon this approach. A direct test of the procedure would to be to compare model channel structures with those determined experimentally. Unfortunately, experimentally determined CFP channel structures are as yet unavailable. A less direct test is to use models to predict the functional (i.e. electrophysiological) properties of "mutant" CFPs, and to compare the predicted behaviour with that observed experimentally. It is this latter approach which is currently being pursued.

Our modelling procedure possibly could be refined by using a molecular mechanics energy minimization approach (Oiki et al. 1990; Raghunathan et al. 1990) to arrive at a better helix bundle model. However, this latter approach also is beset with problems, not the least of which is that of discovering a global, rather than a local, energy minimum. Furthermore, it is likely that for such an energy minimization procedure to be fully successful, *all* components of the system (lipids, water, ions), including the trans-bilayer voltage, may have to be included in the calculations. Such a comprehensive treatment of a complex, multi-phase system would present a considerable computational challenge.

It should not be concluded, however, that it is impossible to refine our approach. We are currently exploring a hierarchical method of channel modelling. Firstly, $\theta$ is defined more objectively, either by utilising the hydrophobic moment, or by evaluating $E(\theta)$ vs. $\theta$ for a helical monomer fixed to rotate about a $z$-axis located at a model of a polar/apolar interface. The $E(\theta)$ minimum defines the $\theta$ value used in the initial bundle model. Having thus determined a value of $\theta$, and employing $N$ values derived from functional measurements, minimizing $E(R)$ vs. $R$ determines the optimum $R$ value.

### *$K^+$ profile evaluation*

As noted at the outset of this paper, it is not our intention to estimate permeation profiles for $K^+$ ions moving through CFP channel models. Rather, energy profiles are employed to locate possible interaction sites between ion and channel. In this respect, our approach resembles those of Furois-Corbin and Pullman (1986) and, in a somewhat different context, of Goodford (1985). The difference lies in the expressions used for the interaction energy. The former group employ:

$$E_T = E_V + E_E + E_P$$

where $E_P$ is a polarisation energy term. Goodford's GRID program uses:

$$E_T = E_V + E_E + E_H$$

where $E_H$ is a hydrogen bond energy term. It also incorporates a rather more complex dielectric model than the current approach in the evaluation of electrostatic energies.

When calculating electrostatic energies we have employed a distance dependent dielectric, $\varepsilon = \varepsilon_0 r$, as is commonly used in molecular mechanics and molecular dynamics studies. This model provides a dielectric close to the free space value at small atomic separations, which increases as the separation increases. There has been some criticism of the use of this approximation when investigating the electrostatic properties of proteins (Rogers 1986; Warshel and Åqvist 1989). Gilson and Honig (1988) made a detailed comparison of different methods of calculating the energetics of charge-charge interactions in proteins. They concluded that a distance dependent dielectric overestimates weak electrostatic interactions, but is less inaccurate for strong interactions. On the basis of the energy minimization studies of Whitlow and Teeter (1986) they suggested that $\varepsilon = 4\varepsilon_0 r$ might be a better approximation.

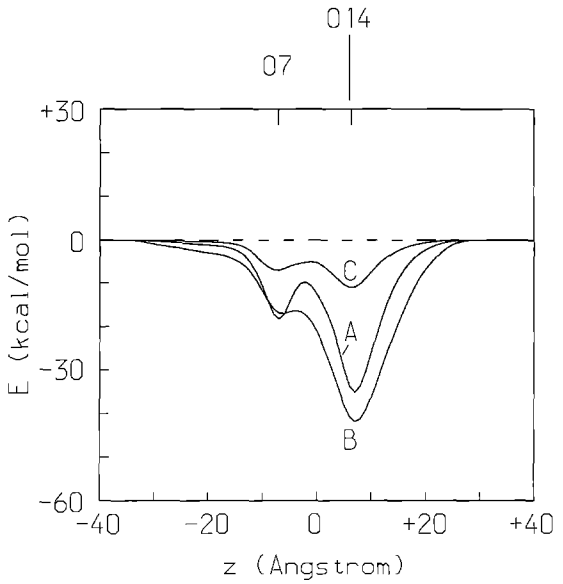


**Fig. 11.** $K^+$ profiles for Zrv-A1–16 model A $N=4$ bundle, obtained using different expressions for the dielectric constant in the evaluation of $E_E$. The dielectric constants used were: (*A*) $\varepsilon=\varepsilon_0 r$; (*B*) $\varepsilon=4\varepsilon_0$; and (*C*) $\varepsilon=4\varepsilon_0 r$

In the light of such criticism, we examined the effect of varying the dielectric on the $K^+$ profile for the Zrv-A1–16 model A, $N=4$ bundle. Three dielectrics were used, one constant ($\varepsilon=4\varepsilon_0$, Fig. 11 B) and two distance dependent ($\varepsilon=\varepsilon_0 r$, Fig. 11 A; and $\varepsilon=4\varepsilon_0 r$, Fig. 11 C). A value of 4 for the constant dielectric was chosen as being that frequently quoted for the interior of proteins (Honig et al. 1986). The profiles for $\varepsilon=4\varepsilon_0$ and for $\varepsilon=\varepsilon_0 r$ are very similar, although the minima are more pronounced in the latter. The profile for $\varepsilon=4\varepsilon_0 r$ yields, as expected, lower interaction energies, but retains the same overall shape. We are therefore reasonably confident that our method of identification of potential ion-channel interaction sites is not over-dependent upon the form of the dielectric. A more detailed treatment of electrostatic interactions, e.g. via numerical solution of the Poisson-Boltzmann equation (see e.g. Sharp and Honig 1990), could be included in a refined procedure for $K^+$ profile estimation.

There are several ways in which the evaluation of $K^+$ profiles may be refined. The first is to "unfreeze" the atomic coordinates. For each value of $z$, the ion is allowed to move in the $x\,y$-plane and the atoms of the channel to relax to a local energy minimum. As Furois-Corbin and Pullman (1987) have shown, this generates changes in the details of the resultant energy profile. Preliminary calculations applying this approach to zervamicin-II B (a polar analogue of Zrv-A1–16; Sansom, unpublished results) are promising, and further studies are underway.

The second refinement would be to determine true ion permeation profiles i.e. to include dehydration/rehydration of the permeant ion. This requires explicit representation of the water molecules within the system, either using the Langevin dipole approximation (Warshel and Russell 1984), or via molecular dynamics simulations of the peptide plus water plus ion system (Mackay et al. 1984; Åqvist and Warshel 1989; Roux and Karplus 1991). Eisenman and Alvarez (1991) have compared these two approaches in their studies of ion permeation through models of channel pores. Of course, to obtain a more complete representation of the system would require greater expenditure of computational time.

### *Zervamicin-A1–16*

The principal achievement of the modelling study of Zrv-A1–16 is to rationalize channel formation by such an apolar peptide. The $K^+$ profile calculation predicts that at least the lower conductance Zrv-A1–16 channels (i.e. lower $N$) should be cation selective. Although it has not been possible to measure the ion selectivity of Zrv-A1–16, it is known that the related peptaibol alamethicin exhibits some degree of cation selectivity (Hanke and Boheim 1980; Hall et al. 1984). Profile calculations have proved of particular interest in confirming the possibility then carbonyl oxygens, exposed via proline-induced kinks, act as cation interaction sites when located at the lining of a trans-bilayer channel (Eisenman and Dani 1987).

One may also attempt to discriminate between model A and model B as descriptions of the open state of zervamicin channels. Combining electrophysiological data with simple modelling of channel conductances (Balaram et al. 1991; Sansom 1991) it seems that the lowest conductance level of zervamicin channels corresponds to an $N=4$ helix bundle. Model A permits ion movement through such a bundle, whereas model B impedes ion movement without a substantial conformational change. This suggests that model A may be closer to the underlying channel structure. However, this is far from conclusive, and further modelling and experimental studies are required.

Having established that our modelling strategy may be successfully applied to Zrv-A1–16 channels, the next stage will be to model channel formation by the polar derivative Zrv-II B, on which the bulk of the functional studies have been performed (Balaram et al. 1991; Sansom 1991). The crystal structure of Zrv-II B is unknown. However, three independent structures for the closely related CFP Zrv-Leu (in which W1 of Zrv-II B is replaced by L1) have recently been determined (Karle et al. 1991; Agarwalla et al. 1991). In these the backbone structure of Zrv-A1–16 is retained, although there are variations in the helix kink angle. Thus it should be possible to model the Zrv-II B monomer with reasonable accuracy, taking Zrv-Leu as a starting point, and thus to model Zrv-II B helix bundles. It will be of considerable interest to explore roles of polar sidechains in stabilization of helix bundle formation by intramolecular H-bonding (Nagaraj and Balaram 1981; Fox and Richards 1982), and also to examine the effects of polar sidechains on the $K^+$ profile.

### *δ-Toxin-1–20*

The $N=6$ δ-toxin-1–20 model rationalizes the observed cation selectivity of δ-toxin channels (Mellor et al. 1988). The explanation in terms of three rings of polar residues

available for $M^+$-peptide interactions (Q3, D11, and D18) is a modification of the earlier model, developed using helical wheel projections of the amino acid sequence, in which D4, rather than Q3, was proposed to form the N-terminal ring (Mellor et al. 1988; Sansom 1991).

An omission from the current model is the C-terminal hexapeptide, disordered in the NMR structure, which contains three lysine groups. One might expect these to perturb the C-terminal minimum in the energy profile, rendering it much shallower and narrower, or even to create a C-terminal barrier to cations. There are two possible ways in which the C-terminal region may be modelled. This region may be induced into a helical conformation, thus forming a continuous α-helix for all 26 residues of the peptide when present in the bilayer. This model could be explored using the current approach. Alternatively, the C-terminal tail may remain disordered, in which case molecular dynamics simulations would be required in order to obtain an average $K^+$ profile. Studies are underway to compare these two possibilities.

It is pertinent to compare our model of the δ-toxin channel, composed of *six parallel* α-helices, with the model(s) proposed by Raghunathan et al. (1990) which are constructed from *anti-parallel* helix bundles, stabilised by intramolecular salt-bridges. In the latter class of model, the $N=6$ model has the central pore completely blocked by the sidechains of W15. An $N=8$ model is suggested as the most likely explantion of δ-toxin channel activity. This could (just) be accommodated by the concentration dependence of δ-toxin channel formation (Mellor et al. 1988). However, an anti-parallel (i.e. *cis/trans* symmetric) model seems inherently unlikely given that δ-toxin channels are formed when peptide is added only to the *cis* face of the bilayer. Furthermore, in the anti-parallel $N=8$ model, the net charge lining the channel is zero, and the authors consequently invoke lipid headgroup interactions to explain the observed cation selectivity of δ-toxin channels. Thus, while the situation remains incompletely resolved, the balance of evidence seems to favour the parallel helix bundle model. Of course, this model may be modified to include parallel bundles with different $N$ values in order to explain the observed conductance heterogeneity of δ-toxin channels.

A further interesting feature of the δ-toxin channel model is the potential for occlusion of the channel by flipping of W15 sidechains about their $C\beta$-$C\gamma$ bonds. This might be predicted to result in "flickering" of the open channel to a lower conductance or closed state. Such channel flickering (i.e. brief duration closures) is indeed observed, even in the presence of 3.0 *M* KCl under which conditions the open state of the channel is stabilized. The time constant for δ-toxin channel flickering is of the order of 0.3 ms. Interestingly, ring flipping of Tyr-35 of bovine pancreatic trypsin inhibitor has been studied using both NMR and simulation methods, yielding time constants of 1.7 s and 1.9 ms respectively (discussed in Brooks et al. 1988). Thus the timescale of the observed flickering is broadly compatible with that suggested by studies of protein dynamics. Alouf et al. (1989) have synthesised a "mutant" δ-toxin, in which the tryptophan ring is moved from position 15 to position 16, i.e. the ring is removed to the hydrophobic face of the bilayer. This peptide forms ion channels in planar bilayers (Sansom, Kerr and Dufourcq, unpublished results), and a detailed comparison of the functional properties of the two δ-toxins is underway, alongside a parallel modelling study. This should provide important information on possible roles of sidechain conformational changes in gating of ion channels.

Overall, the studies described have indicated the value of modelling CFPs in conjunction with functional (i.e. planar bilayer) investigations. The latter provide important constraints upon possible models. Once developed, channel models allow one to rationalize single channel properties. Future studies will be directed towards refinement of the modelling procedures, and towards their applications to a wide range of CFPs. In this way it is hoped that some of the rules underlying the construction of ion selective trans-bilayer pores may be elucidated.

*Acknowledgements.* We wish to thank our colleagues Dr. P. Artymiuk, Prof. P. Balaram, Dr. J. Dufourcq and Dr. D. Rice for their interest in this work. Our thanks also to Dr. R. L. Ramsey for invaluable help with computing. This work was supported by grants from the Nuffield Foundation, the SERC, and the Wellcome Trust. IDK is supported by Shell Research Ltd.

## References

Agarwalla S, Mellor IR, Sansom MSP, Karle IL, Flippen-Anderson JL, Uma K, Krishna K, Sukumar M, Balaram P (1991) Zervamicins, a structurally characterised peptide model for membrane ion channels (in preparation)

Alouf JE, Dufourcq J, Siffert O, Thiaudiere E, Geoffroy C (1989) Interaction of staphylococcal δ-toxin synthetic analogues with erythrocytes and phospholipid vesicles. Eur J Biochem 183:381–390

Åqvist J, Warshel A (1989) Energetics of ion permeation through ion channels: solvation of $Na^+$ by gramicidin A. Biophys J 56:171–182

Balaram P, Krishna K, Sukumar M, Mellor IR, Sansom MSP (1991) Properties of ion channels formed by zervamicins (in preparation)

Boheim G, Hanke W, Jung G (1983) Alamethicin pore formation: voltage-dependent flip-flop of α-helix dipoles. Biophys Struct Mech 9:181–191

Brooks BR, Bruccoleri RE, Olafson BD, States DJ, Swaminathan S, Karplus M (1983) CHARMM: a program for macromolecular energy, minimization, and dynamics calculations. J Comp Chem 4:187–217

Brooks CL, Karplus M, Pettitt BM (1988) Proteins: a theoretical perspective of dynamics, structure, and thermodynamics. Wiley, New York

Chatrabarti P (1990) Systematics in the interaction of metal ions with the main-chain carbonyl group in protein structures. Biochemistry 29:651–658

Eisenberg D, Weiss RM, Terwilliger TC (1982) The helical hydrophobic moment: a measure of the amphiphilicity of a helix. Nature 299:371–374

Eisenberg D, Schwarz E, Komaromy M, Wall R (1984) Analysis of membrane and surface protein sequences with the hydrophobic moment plot. J Mol Biol 179:125–142

Eisenman G, Dani JA (1987) An introduction to molecular architecture and permeability of ion channels. Ann Rev Biophys Chem 16:205–226

Eisenman G, Alvarez O (1991) Structure and function of channels and channelogs as studied by computational chemistry. J Membrane Biol 119:109–132

Fitton JE (1981) Physicochemical studies on delta haemolysin, a Staphylococcal cytolytic peptide. FEBS Lett 130:257–260

Fox RO, Richards FM (1982) A voltage-gated ion channel model inferred from the crystal structure of alamethicin at 1.5 Å resolution. Nature 300:325–330

Furois-Corbin S, Pullman A (1986) Theoretical study of the packing of α-helices by energy minimization: effect of the length of the helices on the packing energy and on the optimal configuration of a pair. Chem Phys Lett 123:305–310

Furois-Corbin S, Pullman A (1987) Theoretical study of potential ion channels formed by a bundle of α-helices: effect of the presence of polar residues along the inner channel wall. J Biomol Struct Dyn 4:589–597

Furois-Corbin S, Pullman A (1989a) A possible model for the inner wall of the acetylcholine receptor channel. Biochim Biophys Acta 984:339–350

Furois-Corbin S, Pullman A (1989b) Energy profiles in the acetylcholine receptor (AChR) channel. FEBS Lett 252:63–68

Furois-Corbin S, Pullman A (1991) The effect of point mutations on energy profiles in a model of the nicotinic acetylcholine receptor (AChR) channel. Biophys Chem 39:153–159

Gilson MK, Honig BH (1988) Energetics of charge-charge interactions in proteins. Proteins: Struct Funct Genet 3:32–52

Goodford PJ (1985) A computational procedure for determining energetically favorable binding sites on biologically important macromolecules. J Med Chem 28:849–857

Hall JE, Vodyanoy I, Balasubramanian TM, Marshall GR (1984) Alamethicin: a rich model for channel behaviour. Biophys J 45:223–247

Hanke W, Boheim G (1980) The lowest conductance state of the alamethicin pore. Biochim Biophys Acta 596:456–462

Hol WG, von Duijen PT, Berendsen HJC (1978) The α-helix dipole and the properties of proteins. Nature 273:443–446

Honig BH, Hubbell WL, Flewelling RF (1986) Electrostatic interactions in membranes and proteins. Ann Rev Biophys Chem 15:163–193

Karle IL, Flippen-Andersen J, Sukumar M, Balaram P (1987) Conformation of a 16-residue zervamicin II A analog peptide containing 3 different structural features: $3_{10}$-helix, α-helix and β-bend ribbon. Proc Natl Acad Sci USA 84:5087–5091

Karle IL, Flippen-Anderson JL, Agarwalla S, Balaram P (1991) Crystal structure of Leu-zervamicin, a membrane ion channel peptide. Implications for gating mechanisms. Proc Natl Acad Sci USA 88:5307–5311

Krishna K, Sukumar M, Balaram P (1990) Structural chemistry and membrane modifying activity of the fungal polypeptides zervamicins, antiamoebins and efrapeptins. Pure Appl Chem 62:1417–1420

Lee KH, Fitton JE, Wüthrich K (1987) Nuclear magnetic resonance investigation of the conformation of δ-haemolysin bound to dodecylphosphocholine micelles. Biochim Biophys Acta 91:144–153

Mackay DHJ, Berens PH, Wilson KR, Hagler AT (1984) Structure and dynamics of ion transport through gramicidin A. Biophys J 46:229–248

Mellor IR, Thomas DH, Sansom MSP (1988) Properties of ion channels formed by *Staphylococcus aureus* δ-toxin. Biochim Biophys Acta 942:280–294

Nagaraj R, Balaram P (1981) Alamethicin, a transmembrane channel. Acc Chem Res 14:356–362

Oiki S, Madison V, Montal M (1990) Bundles of amphipathic transmembrane α-helices as a structural motif for ion-conducting channel proteins: studies on sodium channels and acetylcholine receptors. Proteins: Struct Funct Genet 8:226–236

Raghunathan G, Seetharamulu P, Brooks BR, Guy HR (1990) Models of δ-hemolysin membrane channels and crystal structures. Proteins: Struct Funct Genet 8:213–225

Rogers NK (1986) The modelling of electrostatic interactions in globular proteins. Prog Biophys Mol Biol 48:37–66

Roux B, Karplus M (1991) Ion transport in a model gramicidin channel. Biophys J 59:961–981

Sansom MSP (1991) The biophysics of peptide models of ion channels. Prog Biophys Mol Biol 55:139–236

Sansom MSP, Mellor IR (1990) Analysis of single ion channel gating using current-voltage surfaces. J Theor Biol 11:213–223

Sharp KA, Honig B (1990) Electrostatic interactions in macromolecules: theory and applications. Ann Rev Biophys Chem 19:301–332

Tappin MJ, Pastore A, Norton RS, Freer JH, Campbell ID (1988) High resolution $^1$H NMR study of the solution structure of δ-hemolysin. Biochemistry 27:1643–1647

Thomas DH, Rice DW, Fitton JE (1986) Crystallization of the delta toxin of *Staphylococcus aureus*. J Mol Biol 192:675–676

Vogel H (1987) Comparison of the conformation and orientation of alametticin and melittin in lipid membranes. Biochemistry 26:4562–4572

Warshel A, Åqvist J (1989) Electrostatic correlation of structure and function in proteins. Chim Scr 29A:75–83

Warshel A, Russell ST (1984) Calculations of electrostatic interactions in biological systems and in solutions. Q Rev Biophys 17:283–422

Whitlow M, Teeter MM (1986) An empirical examination of potential energy minimization using the well-determined structure of the protein crambin. J Am Chem Soc 108:7163–7172